ACS OMEGA

Open Access

http://pubs.acs.org/journal/acsodf

Article

Short Antiangiogenic MMP-2 Peptide-Decorated Conjugated Linoleic Acid-Coated SPIONs for Targeted Paclitaxel Delivery in an A549 Cell Xenograft Mouse Tumor Model

Lindokuhle M. Ngema, Samson A. Adeyemi, Thashree Marimuthu, Philemon N. Ubanako, Wilfred Ngwa, and Yahya E. Choonara*

Cite This: *ACS Omega* 2024, 9, 700−713

Read Online

ACCESS | Metrics & More | Article Recommendations

ABSTRACT: The design of targeted antiangiogenic nanovectors for the delivery of anticancer drugs presents a viable approach for effective management of nonsmall-cell lung carcinoma (NSCLC). Herein, we report on the fabrication of a targeted delivery nanosystem for paclitaxel (PTX) functionalized with a short antimatrix metalloproteinase 2 (MMP-2) CTT peptide for selective MMP-2 targeting and effective antitumor activity in NSCLC. The fabrication of the targeted nanosystem (CLA-coated PTX-SPIONs@CTT) involved coating of superparamagnetic iron-oxide nanoparticles (SPIONs) with conjugated linoleic acid (CLA) via chemisorption, onto which PTX was adsorbed, and subsequent surface functionalization with carboxylic acid groups for conjugation of the CTT peptide. CLA-coated PTX SPIONs@CTT had a mean particle size of 99.4 nm and a PTX loading efficiency of ∼98.5%. The nanosystem exhibited a site-specific in vitro PTX release and a marked antiproliferative action on lung adenocarcinoma cells. The CTT-functionalized nanosystem significantly inhibited MMP-2 secretion by almost 70% from endothelial cells, indicating specific anti-MMP-2 activity. Treatment of tumor-bearing mice with subcutaneous injection of the CTT-functionalized nanosystem resulted in 69.7% tumor inhibition rate, and the administration of the nanosystem subcutaneously prolonged the half-life of PTX and circulation time in vivo. As such, CLA-coated PTX-SPIONs@CTT presents with potential for application as a targeted nanomedicine in NSCLC management.

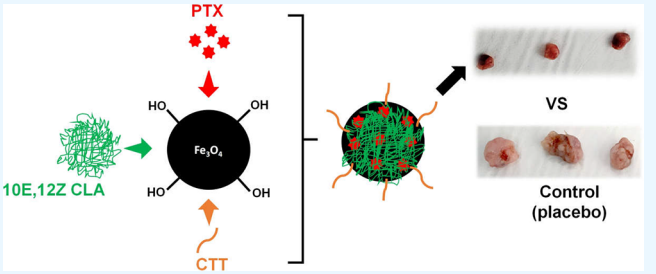

INTRODUCTION

Nonsmall-cell lung carcinoma (NSCLC) remains a global burden[1] owing to plateaued treatment modalities currently available, including combinational chemotherapy, which presents with undesired cytotoxic side effects due to non-specificity.[2] Recently, nanotechnology and its application in nanomedicine has gained major recognition in the development of nanobased therapeutics for NSCLC.[2] As such, new therapeutic interventions for NSCLC are being devised, and the focus is currently on targeted nanomedicines with high specificity, minimal side effects, and smaller size for tumor penetration.[3,4]

Interestingly, angiogenesis targeting presents a potentially viable therapeutic intervention for NSCLC.[5] Angiogenesis is fundamental in the proliferation and metastasis of tumor cells as a key provider of nutrients and oxygen.[6] Hence, the inhibition of tumor angiogenesis pathways is a prospective therapeutic approach for NSCLC. Synthetic and natural angiogenesis inhibitors which block new blood vessel formation have been explored for tumor therapy,[7] and some peptide-based inhibitors have demonstrated promising anti-angiogenic activity.[8−10] Matrix metalloproteinase 2 (MMP-2) has been shown to be implicated in lung cancer angiogenesis regulation and tumor metastasis.[11,12] MMP-2 expression is linked to tumor-induced angiogenesis, where it is responsible for degrading the extracellular matrix (ECM) and releasing stored angiogenic factors (i.e., basic fibroblast and/or vascular endothelial growth factors) which propel angiogenesis, tumor differentiation, and metastasis.[13,14] Thus, targeting MMP-2 and downregulating its expression could halt tumor angiogenesis and suppress proliferation and metastasis.

Accordingly, CTT peptide (CTTHWGFTLC) is an MMP-2 selective inhibitory peptide with reported antiangiogenic activity.[15] CTT is a cyclic peptide (∼1.17 kDa) shown to suppress MMP-2 and significantly block angiogenesis and migration of endothelial and cancerous cells.[16,17] Primarily,

Received: August 30, 2023
Revised: October 28, 2023
Accepted: October 31, 2023
Published: December 22, 2023

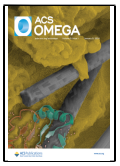

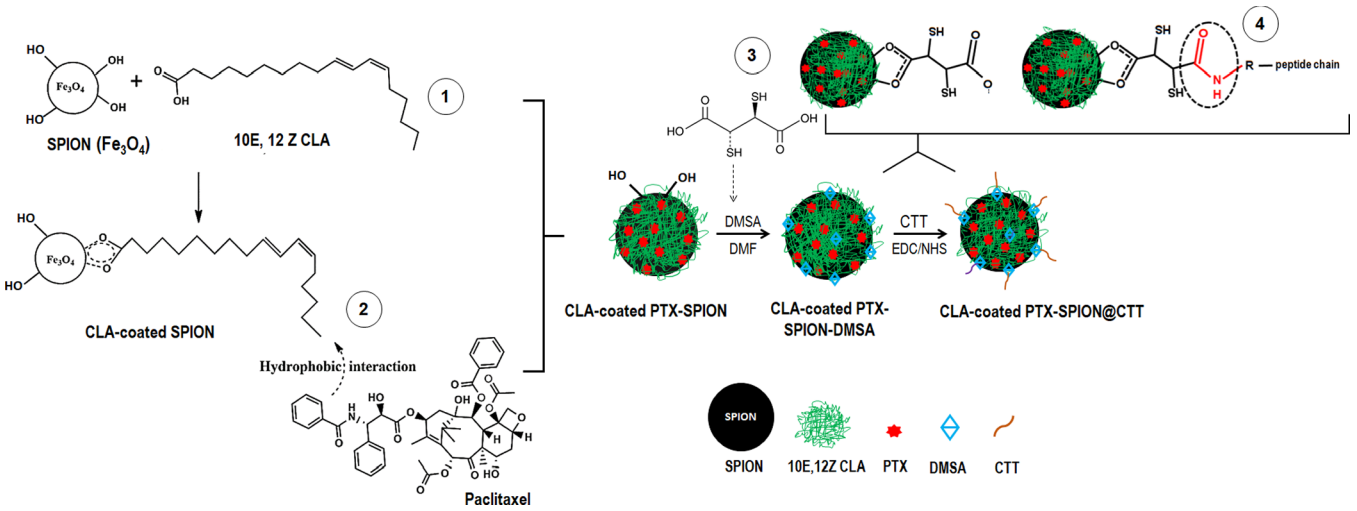

Figure 1. Step-wise formulation of CLA-coated PTX-SPIONs@CTT (CTT nanosystem). Step 1 is the chemisorption (coating) of 10E, 12Z CLA onto SPIONs. Step 2 is self-assembled loading of PTX via spontaneous hydrophobic interaction with 10E, 12Z CLA ends. Step 3 is −COOH functionalization using DMSA (DMF facilitates the reaction between SPIONs −OH and DMSA through hydrogen bonding). Step 4 is the final conjugation of CTT onto activated $-COO^-$ via its terminal $-NH_2$ group, facilitated by EDC/NHS. The conjugation of CTT results in amide II bond formation and a growing peptide chain.

CTT selectively binds MMP-2 and blocks the endothelial cells from degrading and remodeling the adjacent ECM, leading to the disruption of neovascularization and ultimately tumor growth regression.[16] The selective targeting ability of CTT has been leveraged to design targeted liposomal drug-delivery nanosystems for other cancers, such as ovarian cancer and fibrosarcoma, for targeting MMP-2 and MMP-9.[18] However, no studies have explored the similar application of CTT in NSCLC targeted therapy; thus, it was a suitable choice for this investigation for targeting MMP-2 and halting tumor angiogenesis. Evidently, various nanosystems that have been investigated for drug delivery in NSCLC therapy are mainly affected by nonspecificity, physicochemical instability, poor bioavailability, and adverse drug effects, leading to poor therapeutic efficacy.[2,19] As such, our CTT nanosystem was set to overcome these challenges.

Previously, we formulated and characterized a nanosystem comprising superparamagnetic iron oxide nanoparticles (SPIONs) coated with *trans*-10, *cis*-12 conjugated linoleic acid (10E, 12Z CLA) and loaded with paclitaxel (PTX) (self-assemble) to yield a potent PTX nanovector which exhibited enhanced PTX killing effect in lung adenocarcinoma cell lines.[20] SPIONs are excellent nanovectors with desirable smaller size (<100 nm) and are easy to functionalize.[21] Meanwhile, the natural fatty acid 10E, 12Z CLA presents with anticancer benefits[22] and allows partitioning of hydrophobic anticancer drugs like PTX for enhanced bioavailability and antiproliferative activity.[20] As such, in the present study, we functionalized a CLA-coated PTX nanovector with the CTT peptide via a series of favorable chemical reactions involving carboxylic acid decoration and coupling chemistry to yield CLA-coated PTX-SPIONs@CTT (CTT nanosystem) and conducted in vitro analyses to show antiangiogenic and antiproliferative activities in endothelial cells and lung adenocarcinoma cells, respectively, and lung tumor targetability in the established lung xenografts in nude mice following subcutaneous (SC) injection.

RESULTS AND DISCUSSION

Formulation of CLA-Coated PTX-SPIONs@CTT (CTT Nanosystem). The SPIONs, as the core of the nanoformulation, were efficiently synthesized using a coprecipitation method, yielding black Fe_3O_4 nanoparticles with a mean hydrodynamic size of ∼51 nm. The working conditions involved in the coprecipitation method, including inert atmosphere and high temperature, were instrumental in attaining the desired smaller size, morphology, and distribution of the particles while limiting oxidation.[20,23] The overall formulation scheme of the CTT nanosystem is depicted in Figure 1 (step 1−4). The coating of the SPION surface with 10E, 12Z CLA was successfully achieved, owing to the availability of the hydroxyl (−OH) groups on SPIONs and the carboxyl groups (−COOH) on CLA, allowing chemisorption. The chemisorption of fatty acids such as linoleic acid, oleic acid, palmitic acid, and glycerol monooleate onto SPIONs is a well-established phenomenon that has been widely reported.[24−26]

Accordingly, about 10.3% of 10E, 12 CLA was found to be coated onto SPIONs. A range of 10−14% fatty acid content on SPIONs has been reported from previous studies, employing thermogravimetric analysis (TGA).[20,24,26] The presence of 10E, 12Z CLA allowed maximal partitioning of PTX, with 98.5% adsorption efficiency, which was likely linked to the hydrophobic nature of 10E, 12Z CLA complementing the hydrophobic nature of PTX, allowing spontaneous hydrophobic−hydrophobic interaction. Meanwhile, the 9.8% drug loading capacity achieved could be likely due to the large surface area of SPIONs,[27] and it is favorable, given that 10% w/w PTX was applied in the formulation. The loading of hydrophobic drugs into nanoparticles is generally challenging;[28] however, in the present work, the choice of 10E, 12Z CLA circumvented the problem. The availability of free −OH groups on SPIONs allowed for further surface functionalization with −COOH moieties from *meso*-2,3-dimercaptosuccinic acid (DMSA) for CTT conjugation. Normally, SPIONs synthesized via coprecipitation present with excess −OH groups.[24]

https://doi.org/10.1021/acsomega.3c06489
ACS Omega 2024, 9, 700−713

A total of 64 per gram free −COOH groups were present on the surface from the 1.6 M DMSA used. The proportion of free −COOH obtained correlates with the concentration of DMSA employed. A related study has reported free −COOH numbers of nearly 8 per gram of the sample when 0.2 M DMSA was employed and noted that the acid numbers increase when the DMSA concentration is increased, until binding saturation is reached.[24] The use of dimethylformamide (DMF), a polar aprotic solvent, favored the DMSA grafting reaction by initiating hydrogen bonding without partaking in the reaction.[29] Also, to avoid displacing the CLA∼PTX complex on the SPION surface, DMF was ideal since the orientation and conformation of bound CLA∼PTX molecules may be energetically stable in DMF, leading to reduced solubility.[24] The −COOH functionalization step was successfully achieved, as well as the conjugation of CTT, yielding CLA-coated PTX-SPIONs@CTT, as evidenced from the comparative Fourier transform infrared (FT-IR) spectral analysis (Figure 3).

Overall Morphological Assessment of the CTT Nanosystem. The surface charge and average particle size and dispersion were, respectively, determined through phase light scattering and dynamic light scattering (DLS), with corresponding recorded data shown in Table 1. Transmission electron microscopy (TEM) further confirmed the respective surface and basic structural morphology of the CTT nanosystem (Figure 2b). A zeta potential of −31.8 ± 0.5 mV and a polydispersity index (PDI) of 0.2 ± 0.01 showed the colloidal stability and reduced aggregation of the formulated CTT nanosystem in aqueous media. Importantly, zeta potential is a good determinant of the colloidal stability of nanoparticle suspensions, with zeta potential values further away from zero, between ±30 and ±40 mV indicative of a stable nanoparticle system.[30] The PDI recorded for the CTT nanosystem was lower than that of pure SPIONs (0.4 ± 0.1) previously reported,[20] indicating the effect of surface coating with 10E, 12Z CLA. Essentially, SPIONs tend to aggregate due to their magnetic behavior and therefore require to be surface-modified to limit aggregation.[31] Various surface-coating agents, including related fatty acids such as oleic and linoleic acids, have been employed to circumvent SPION aggregation.[25,26]

Table 1. Recorded Average Size, Surface Charge, and PDI of CLA-Coated PTX-SPIONs@CTT (CTT Nanosystem) and Pristine SPIONs

	average hydrodynamic size (nm)	zeta potential (mV)	polydispersity index (PDI)
CTT nanosystem	99.4 ± 2.0	−31.8 ± 0.5	0.2 ± 0.1
SPION (before modifications)	51.0 ± 1.3	−24.3 ± 1.3	0.4 ± 0.1

The average hydrodynamic size recorded for the CTT nanosystem was 99.4 ± 2.0 nm (Figure 2a), which is an ideal size for application in NSCLC. It is reported that nanocarriers with a diameter range of 10−100 nm are ideal for lung tumor penetration; meanwhile, carriers above 100 nm may be subject to removal by alveolar macrophages.[32] As such, maintaining a size of not more than 100 nm was crucial in the present study. The size, zeta potential, and PDI deviations were monitored throughout the formulation process and involved modifications (i.e., CLA coating and PTX loading). Accordingly, the size, zeta potential, and PDI of the CLA-coated PTX-SPIONs were 96.5 ± 0.6 nm, −27.3 ± 1.9 Mv, and 0.1 ± 0.02 PDI, respectively. TEM characterization further supported that the size of the final CTT nanoformulation was in the nm range and confirmed that the CTT nanosystem exhibited a quasi-spherical shape (Figure 2b).

TEM analysis was ideal in this regard compared to scanning electron microscopy (SEM) since SEM did not give the best resolution of the nanoparticles. Accordingly, the presented TEM micrograph was captured at 7000× magnification from isolated nanoparticles to clearly show the overall shape. The shape could be associated with carboxylic functionalization with DMSA, through which the DMSA short chains impart a quasi-spherical conformation on iron oxides.[33] It has been reported that the shape of the nanoparticles may influence their cellular uptake and biodistribution,[34] and as such, the quasi-spherical shape of the CTT nanosystem may influence the cellular uptake of the nanosystem.

Evaluation of Chemical Functionality and Transformations toward Formulation of the CTT Nanosystem. The evaluation of chemical functionality of the constituents of the CTT nanosystem and transformations thereof was beneficial in ascertaining the successful formation of the desired CTT nanosystem. FT-IR spectroscopy was chosen as the technique of choice for precise deconvolution of chemical bond transformations toward the formation of CTT nanosystem, owing to its robustness in bond characterization compared to other techniques.[35,36] Importantly, this allowed us to discern the chemistry involved in the formulation of the nanosystem and ultimately verify our fabrication methodology. Accordingly, the spectra from the FT-IR spectroscopy analysis

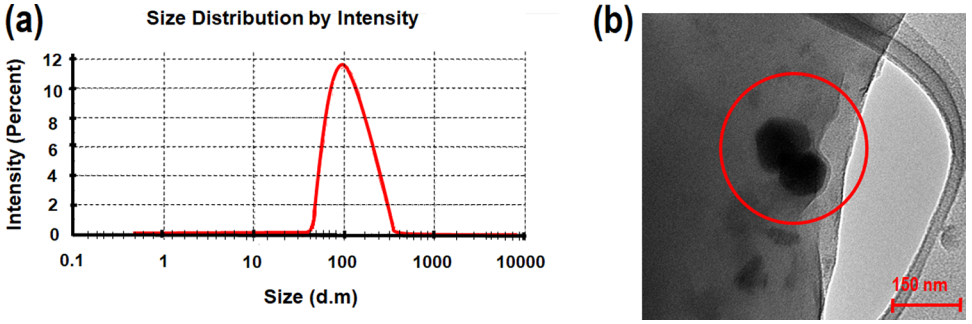

Figure 2. (a) Representation of characteristic physical features of CTT nanosystem depicting the average hydrodynamic size distribution from DLS measurement and (b) TEM micrograph on a scale bar of 150 nm (7000× magnification) showing a quasi-spherical shape of the formulated CTT nanosystem (red circle). The TEM micrograph supported the size measurement from the DLS record, confirming that the particles were in the nm range and <150 nm (within scale bar).

https://doi.org/10.1021/acsomega.3c06489
ACS Omega 2024, 9, 700−713

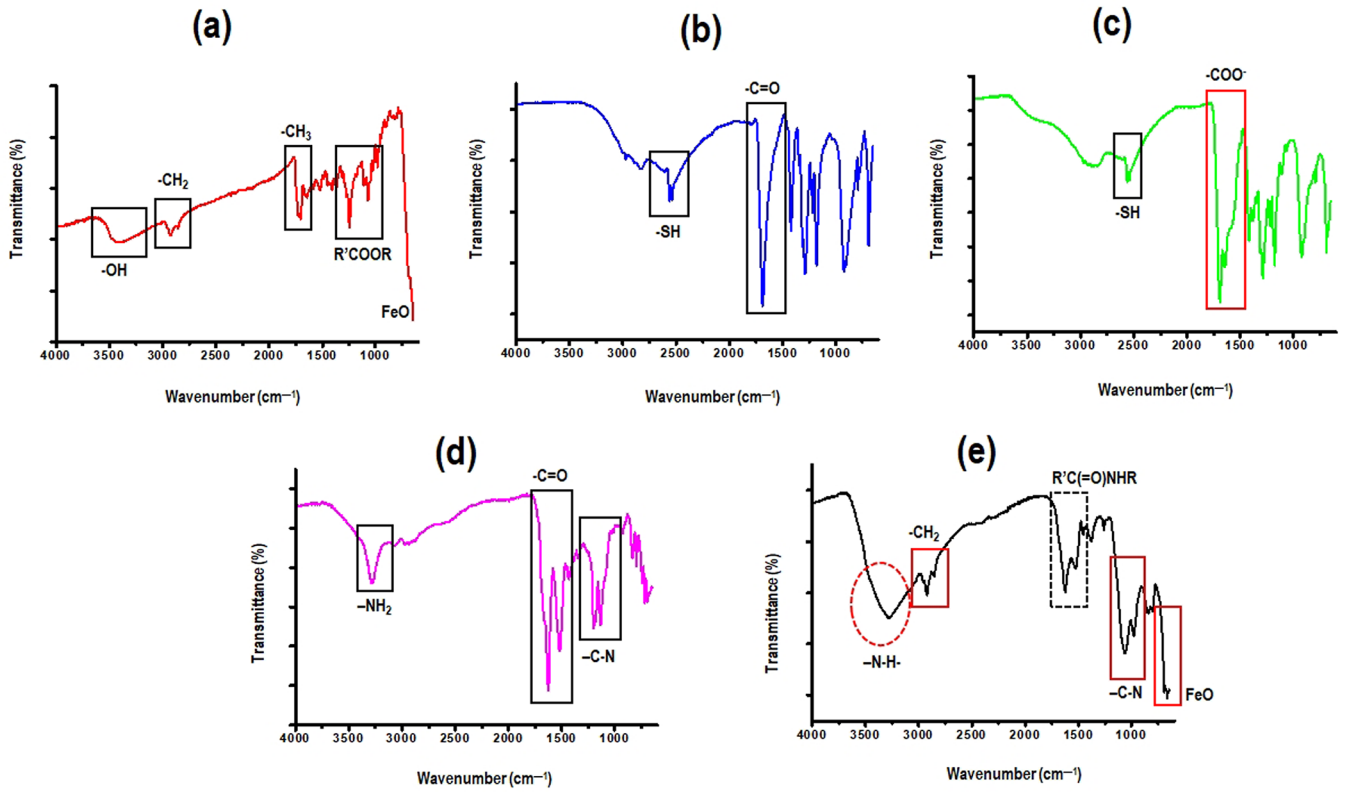

Figure 3. FT-IR spectra showing chemical functionality mappings of (a) CLA-coated PTX-SPIONs, (b) only DMSA, (c) carboxylated (DMSA) CLA-coated PTX-SPIONs, (d) CTT peptide, and (e) final CTT nanosystem.

are presented in Figure 3a−e. The spectra for pristine SPIONs, 10E, 12Z CLA, and pristine PTX can be found from our previous publication.[20] The characteristic peaks of PTX (1244 and 3479 cm^{-1}, attributed to ester and −OH groups, respectively) and those of 10E, 12Z CLA (1403 cm^{-1} and ∼2922−2852 cm^{-1}, belonging to CH_3 bending and symmetrical/asymmetrical CH_2 stretches), as well as iron oxide (FeO = 580 cm^{-1}) were evident in the CLA-coated PTX-SPION spectrum (Figure 3a),[25,37] confirming the coating with 10E, 12Z CLA and PTX loading onto SPIONs.

Likewise, major peaks at 1685 and 2561 cm^{-1} (belonging to −C═O of the carboxyl groups and −SH of the thiol groups, respectively)[38] were present in the spectrum of DMSA (Figure 3b). A split and a shift in the DMSA peak (−C═O) from 1685 cm^{-1} to around 1680−1675 cm^{-1} (red marker) could be seen in a DMSA-functionalized CLA-coated PTX-SPION spectrum (Figure 3c), attributed to carboxylate ion (COO^-) vibrations when DMSA is linked onto SPION surface via the carboxyl group.[38,39] The pure CTT peptide (Figure 3d) exhibited characteristic peaks for terminus primary amine ($-NH_2$ = 3280 cm^{-1}), −C═O stretches (1625, 1518 cm^{-1}), and peptide bond stretch (C−N═1199−1134 cm^{-1}).[40] The conjugation of CTT and the overall formation of the CTT nanosystem was supported (Figure 3e) by the presence of characteristic peaks of all constituents (red rectangular markers) in the spectrum, with a visible amide II bond at ∼1570 cm^{-1} (dotted rectangular marker) emanating from CTT conjugation via $-NH_2$ onto the reactive COO^- from DMSA (Figure 1) and a wide peak at 3278 cm^{-1} (red dotted circle) belonging to the −N−H stretch from the new amide II bond formed from CTT conjugation.

In Vitro Release Profile of PTX from the CTT Nanosystem. The release of PTX from the CTT nanosystem was evaluated over 24 h, and the attained profile is presented in Figure 4. Varying levels of release were recorded at different pH profiles, suggesting smart pH-responsiveness of the nanosystem. Accordingly, a sustained and maximal release of PTX was observed at pH 6.8; meanwhile a comparatively lower release was recorded at physiological pH 7.4. An initial release of nearly 30% (1 h) was recorded at pH 6.8, with a continuous release up to a maximum of 99.2% at 16 h. Contrary, an initial

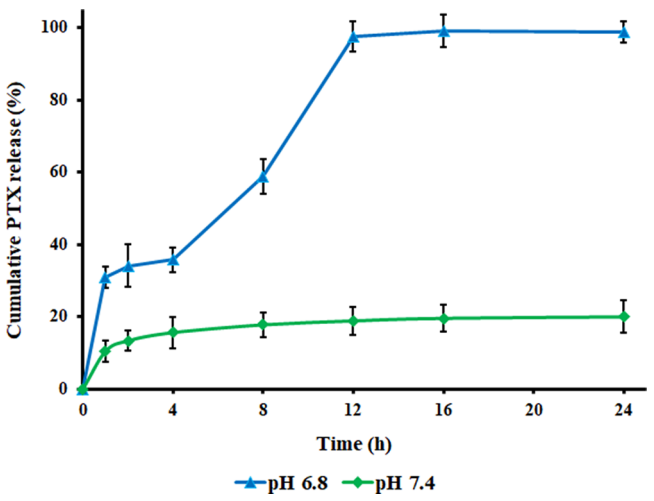

Figure 4. A 24 h PTX release profile at pH 6.8 and pH 7.4. A highly favored release at pH 6.8 could be observed compared to pH 7.4. Data computed as mean ± SD, sampled in triplicates.

https://doi.org/10.1021/acsomega.3c06489
ACS Omega 2024, 9, 700−713

release of only 10.4% PTX could be recorded at pH 7.4, reaching a maximal release of only 19.9% at 24 h, even lesser than that recorded at 1 h at pH 6.8. Essentially, the favored release at pH 6.8 could be associated with breaking of hydrophobic interactions between PTX and CLA at acidic conditions over time. Related studies have reported similar observations when PTX was loaded onto hydrophobic oleic acid and glycerol monooleate and found that hydrophobic interactions are not permanent and are rapidly weakened at acid pH.[24,41]

Evaluation of Antiproliferative Activity of the CTT Nanosystem from the A549 Cell Viability Study. The antiproliferative effect of the CTT nanosystem on A549 cells was ascertained by the determination of viable cells post treatment. Figure 5 presents the viability assessment at

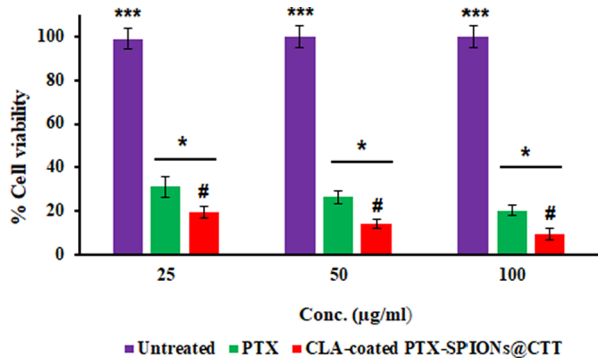

Figure 5. Viability assessement of A549 cells at predetermined treatment concentrations of CLA-coated PTX-SPIONs@CTT (CTT nanosystem) and PTX (positive control). Cell viability (%) was computed after 72 h of incubation and is shown as mean ± SD of triplicate analyses. (*** denotes $p < 0.001$, statistically significant against treatment groups, * denotes $p < 0.05$, statistical significance between PTX and CTT nanosystem at specified concentrations, and # denotes $p < 0.05$, statistical significance among CTT nanosystem concentrations).

different concentrations. A concentration-dependent antiproliferative activity was recorded, attaining % cell viability of 18.5, 15.2, and 12.4% at 25, 50, and 100 μg/mL, respectively. A decline in the number of viable cells with an increase in the treatment concentration is representative of a potent anticancer medicine and correlates with previous studies that have reported a dose-dependent cellular cytotoxicity from various PTX nanoformulations in NSCLC.[42,43] The cell viability data obtained are comparable to the findings from our previous study, where CLA-coated PTX-SPIONs were shown to improve the antiproliferative effect of pristine PTX by almost 3 folds,[20] and the similar experiments were repeated in the present study, with pristine PTX as a positive control exhibiting % cell viability of 31.2, 26.5, and 20.2% at corresponding 25, 50, and 100 μg/mL concentrations, respectively.

In contrast, the % cell viabilty from the CTT nanosystem was found to be <20% at all specified concentrations. The low % cell viability recorded translate to the enhanced antiproliferative action of the CTT nanosystem. Moreover, the IC_{50} for the CTT nanosystem after 72 h exposure was computed to be 0.58 μg/mL, and for pristine PTX, it was 0.96 μg/mL. This supported the significantly increased antiproliferative activity of the CTT nanosystem compared to PTX. Likewise, an IC_{50} of 0.9 μg/mL has been previously recorded for PTX on A549 cells, indicative of the comparable cytotoxicity of the tested PTX in the present study.[44]

Cellular Uptake of the CTT Nanosystem by A549 Cells. A good cellular uptake of the CTT nanosystem by the A549 cells was observed. The cells were identified through nuclei visualization by DAPI staining (blue fluorescence) (Figure 6a), and CLA-coated PTX-SPIONs@CTT were tracked through fluorescein 5(6)-isothiocyanate (FITC) excitation (green fluorescence) as they were labeled with the probe (Figure 6b). A high accumulation of CLA-coated PTX-SPIONs@CTT (green fluorescence) closest to the nuclei (blue fluorescence) compellingly indicated uptake of the nanoformulation by the cells (Figure 6c). This was qualitatively higher than the uptake observed from the nonfunctionalized nanosystem (without CTT) (Figure 6d). The high uptake of the CTT nanosystem by A549 cells could be presumed to emanate from the affinity of CTT to the proteolytic MMP-2 enzyme secreted by the migrating cells, allowing the nanosystem to recognize and penetrate the cells.[45] Meanwhile, the limited uptake observed from the nonfunctionalized nanosystem could be primarily due to the lack of targeting ability. Additionally, the high cellular uptake observed in the present study could be directly linked to improved antiproliferative action demonstrated by the formulated CTT nanosystem on A549 cells (Figure 5). Accordingly, a sufficient concentration of the nanosystem was internalized and reached the nuclei of A549 cells, eliciting cytotoxic effects on the nuclei and resulting in cellular death. Some studies report nuclei rupture as a common event when sufficient cytotoxic agents are taken up by cancerous cells and reach the nuclei.[8,43]

Assessment of MMP-2 Targeting and Secretion Levels by ELISA. Secretion levels of MMP-2 by human dermal microvascular endothelial (HMEC-1) cells were detected and quantified from the cell culture media using a human MMP-2 ELISA kit. The endothelial cells were appropriate for this study as they are involved in blood vessel formation and secretion of signal factors involved in angiogenesis, such as MMP-2.[13] Presented in Figure 7 is the MMP-2 concentration plot from untreated cells as well as cells treated with antiangiogenic peptide functionalized (CTT nanosystem) and nonfunctionalized (CLA-coated PTX-SPIONs) nanoformulations. A highest MMP-2 concentration (1.68 ng/mL) was recorded from untreated cells; meanwhile, the lowest concentration (0.47 ng/mL) was recorded from cells incubated with the formulated CTT nanosystem. Incubation with CLA-coated PTX-SPIONs resulted in concentration levels of 1.55 ng/mL. Higher MMP-2 secretion levels could be expected from untreated cells, indicative of normal uninterrupted endothelial cell growth. Endothelial cells secrete MMP-2 to facilitate the removal of matrix barriers and initiate signaling pathways that promote cell growth, including angiogenesis.[11,46]

A significant variation in MMP-2 secretion levels between cells treated with the CTT nanosystem and cells treated with CLA-coated PTX-SPIONs was an interesting revelation. Essentially, the nonfunctionalized CLA-coated PTX-SPIONs were solely employed for comparison with CLA-coated PTX-SPIONs@CTT to discern the activity of the CTT peptide on MMP-2 targeting. Accordingly, the lower MMP-2 secretion levels recorded from the CTT nanosystem treatments compellingly confirmed the MMP-2 targeting ability of the peptide, resulting in MMP-2 arrest at active sites and

https://doi.org/10.1021/acsomega.3c06489
ACS Omega 2024, 9, 700−713

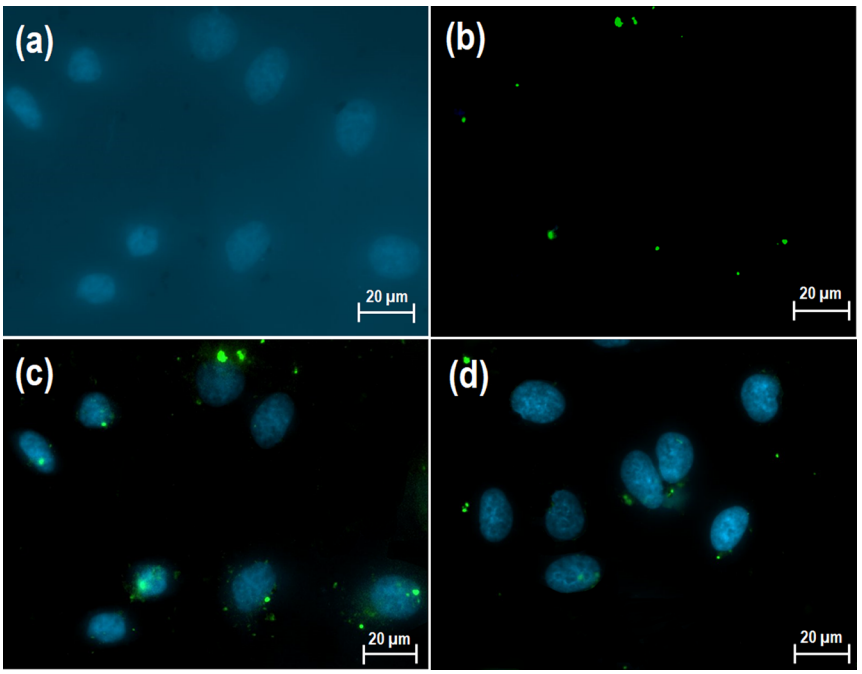

Figure 6. Visualization of cellular uptake and internalization by A549 cells. Micrograph (a) shows nuclei of A549 cells as visualized by DAPI staining and (b) shows CTT nanosystem (FITC-labeled) tracking, while (c) is the overlay of (a, b) showing the cellular uptake of the formulated CTT nanosystem, and (d) is the cellular uptake of the nonfunctionalized (without CTT) nanosystem. The difference in the uptake of the CTT nanosystem (c) vs nonfunctionalized nanosystem (d) is attributed to the lack of MMP-2 targetability in the latter. The untreated control cells were also visualized, showing only the nuclei of cells (data not presented).

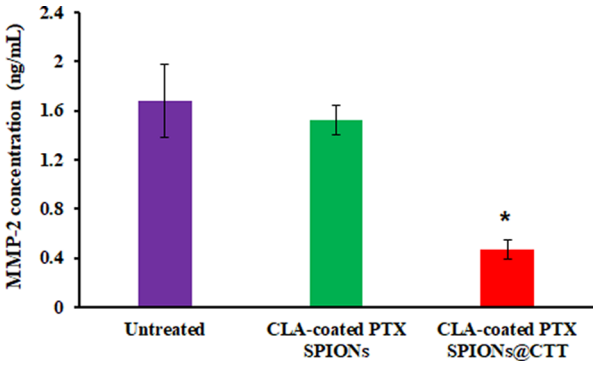

Figure 7. MMP-2 secretion levels from HMEC-1 incubated without and with CLA-coated PTX-SPIONs, and CTT nanosystem quantified by the ELISA kit. Data are presented as mean ± SD (* denotes $p < 0.05$ against CLA-coated PTX-SPIONs and untreated).

inactivation of these endopeptidases that would promote angiogenesis under normal circumstances and tumor angiogenesis in cancers. Meanwhile, nonfunctionalized CLA-coated PTX-SPION treatments yielded elevated MMP-2 levels, which were comparable with untreated control cells, indicating that the nanoformulation had negligible effect on MMP-2 secretion. However, a slight change to 0.92 ng/mL could be the result of cells experiencing mild shock from the introduction of a foreign substance (CLA-coated PTX-SPIONs).

MMPs are largely implicated in cancer as an enabler of tumor angiogenesis.[11] Generally, inhibitors of MMPs, both endogenous and synthetic, have been studied on various cancers and shown to suppress angiogenic responses in vitro and in vivo.[46−48] However, most of these inhibitors are only selective for a general class of MMPs and lack specificity for individual MMP family members.[47] Therefore, a better understanding of specific MMPs and corresponding inhibitors with precise targeting capabilities has been called for in antiangiogenic approaches. Likewise, in this study, we have identified and demonstrated in an endothelial cell line (HMEC-1) that CTT is a potent and specific MMP-2 inhibitor. Although this has been achieved in vitro, an in vivo evaluation of MMP-2 secretion levels would be ideal to further substantiate the MMP-2 targetability of the CTT nanosystem.

Antitumor Activity of the CTT Nanosystem on a Lung Tumor Xenograft Mouse Model. Evaluation of the antitumor activity of the formulated CTT nanosystem was successfully carried out on the developed SC lung tumor xenograft nude mouse model. Nude mice are generally considered ideal for the development of cancer models since they present with a compromised immune system with increased susceptibility to tumor formation.[10,49] In the present study, tumors could be visualized as early as 20 days post inoculation. The recorded tumor volumes (mm^3) post treatment are presented in Figure 8a. Expectedly, tumors from the control mice that received only phosphate-buffered saline (PBS) exhibited enormous growth and reached 1484.7 mm^3 at the end of the study. The enormous growth could be associated with the robustness of A549 cells.[49]

Meanwhile, tumors from mice treated with the CTT nanosystem had their growth significantly regressed compared to all other groups.

A tumor growth inhibition rate (%TGI) of 69.7% was recorded from tumor-bearing mice treated with the CTT nanosystem. Treatment with nonfunctionalized CLA-coated PTX-SPIONs also showed a promising antitumor activity, with %TGI of 52.8%. Contrarily, treatment with comparator Taxol resulted in mild regression with %TGI of only 26.3%. A vivid depiction of growth differences in tumors from the mice is

https://doi.org/10.1021/acsomega.3c06489
ACS Omega 2024, 9, 700−713

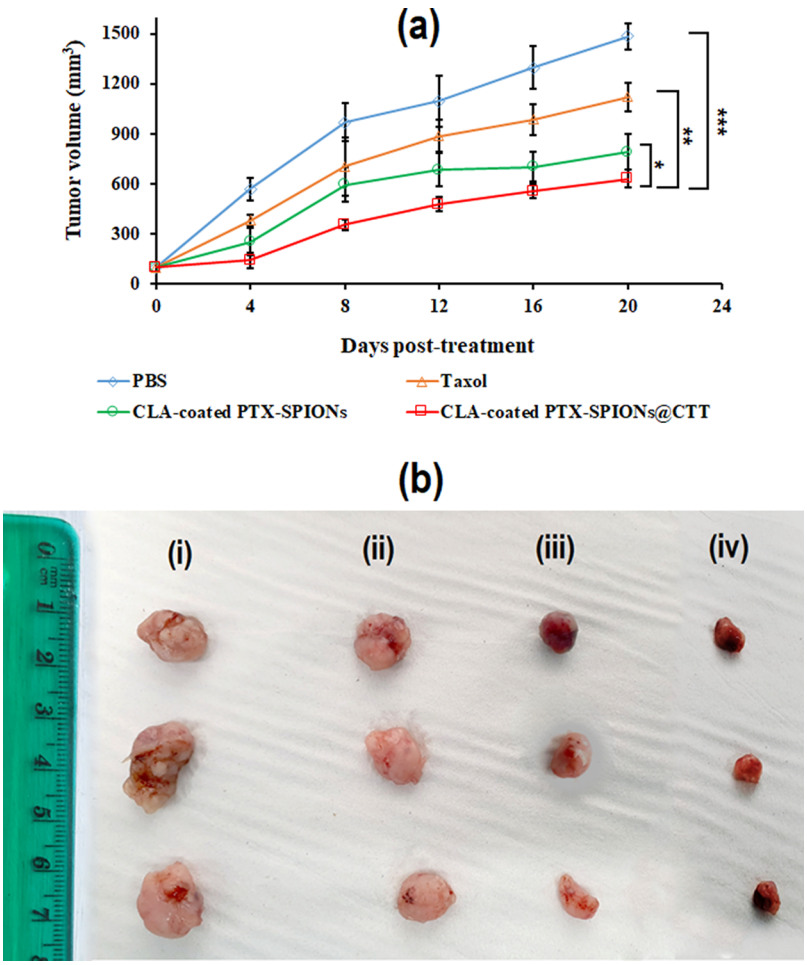

Figure 8. Assessment of antitumor activity depicted by (a) tumor volumes and (b) excised tumors at the end of the study, where (i) are tumors from the PBS cohort, (ii) Taxol cohort, (iii) CLA-coated PTX-SPIONs cohort, and (iv) CTT nanosystem cohort. In frame (a), days 0, 4, 8, and 12 are treatment cycles (1−4) and days 16 to 20 are the observation period. Tumor images in frame (b) clearly shows the variation in sizes corresponding to growth inhibition in vivo. (Data displayed as mean ± SD of sample size $n = 3$, where * denotes $p < 0.05$, ** is $p < 0.01$, and *** is $p < 0.001$).

Table 2. Weight Measurements from Tumored Mice at the Beginning of Treatment Until the End of the Study[a]

	groups[b]			
days	PBS	Taxol	CLA-coated PTX-SPIONs	CTT nanosystem
0	24.39 ± 0.13	24.36 ± 0.12	24.19 ± 0.21	24.24 ± 0.19
4	24.26 ± 0.19	24.28 ± 0.26	24.83 ± 0.35	25.16 ± 0.16
8	23.66 ± 0.35	24.25 ± 0.19	24.65 ± 0.31	25.12 ± 0.13
12	23.86 ± 0.31	23.73 ± 0.22	24.79 ± 0.25	24.64 ± 0.39
16	23.09 ± 0.28	23.83 ± 0.20	24.36 ± 0.46	25.04 ± 0.50
20	23.00 ± 0.27**	24.39 ± 0.31	25.68 ± 0.32	25.76 ± 0.10

[a]Values are Mean ± SD, $n = 3$ (mice exhibiting 10% and more weight loss would be removed from the study as per ethical guidelines). [b]** $p < 0.01$, statistically significant weight loss compared to day 0.

presented in Figure 8b, where excised tumors were visually compared and assessed for growth inhibition. The relatively high antitumor activity of the CTT nanosystem is attributed to tumor targetability conferred by the CTT peptide, which suppresses MMP-2 activity and halts signaling of angiogenesis, thus preventing rampant growth of tumors. Additionally, the combined anti-MMP2 activity with antimitotic activity of PTX presented by the CTT nanosystem is responsible for the observed tumor regression.

Similarly, the promising antitumor activity of CLA-coated PTX-SPIONs is associated with the enhanced PTX anticancer activity conferred by the nanosystem. Essentially, an adequate therapeutic dose of PTX can reach the tumor microenvironment and penetrate tumors via the nanosystem to elicit antimitotic activity and prevent tumors from rapidly dividing. Previously, we had reported that CLA-coated PTX-SPIONs enhance PTX antiproliferative action in vitro,[20] and the current findings support these claims as per the results obtained in the A549 cell xenograft mouse model. Although Taxol did not demonstrate significant antitumor activity, the dosage employed was shown to be tolerated as no eminent side effects, such as major weight loss, were observed during the

https://doi.org/10.1021/acsomega.3c06489
ACS Omega 2024, 9, 700−713

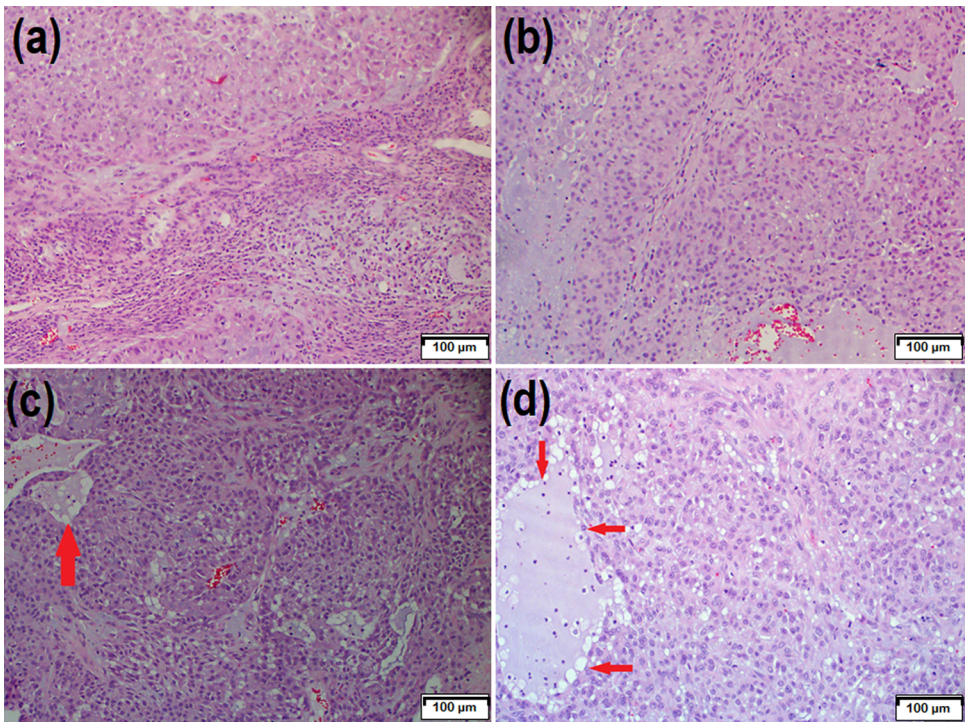

Figure 9. Histopathological assessment of tumors from (a) PBS control mice and mice that received treatment with (b) PTX, (c) CLA-coated PTX-SPIONs, and (d) CTT nanosystem. Tumor sections (c,d) show neoplastic degeneration (red arrows) emanating from treatment with our nanoformulations, more pronounced from treatment with the CTT nanosystem. Micrographs captured at 100 μm plane, 6.3× magnification, H&E stain.

study. Essentially, the maximum tolerated dose of Taxol has been determined to be 20 mg/kg.[50] Commonly, the overall weight loss from the adipose tissue and the skeletal muscle is a primary indicator of manifestation of cancer and a side effect reported from chemotherapy in mice studies.[10,36,51] Presented in Table 2 are the recorded body weights throughout the study. A control group (PBS) exhibited significant weight loss (∼5%) toward the end of the study due to rapid progression of the cancer.

Histopathological Analysis of Tumors from Treated and Untreated Mice. A histopathological analysis of tumors was primarily carried out to assess any structural variations afforded by different treatments and further discern organelles possibly affected by the treatments. Presented in Figure 9 are micrographs of tissue sections of tumors from the PBS, Taxol, CLA-coated PTX-SPION, and CTT nanosystem cohorts. A multifocal inflammation around muscle fibers, linked to aggressive tumor growth, was observed in tumors from the PBS cohort (Figure 9a). Inflammation is often associated with promoting various stages of tumorigenesis,[52] and such could be inferred from the obtained micrographs. Additionally, about 29 mitosis could be identified from the tumor in 10-high-power-fields/2.37 mm^2. Tumors from Taxol-treated mice presented with a cystic space and scattered loose blood cells with a decreased mitosis count of 17 identifiable mitosis in high-power-fields (Figure 9b). The slight reduction in mitosis count could be associated with PTX antimitotic activity and correlates with the mild tumor regression observed from PTX treatment in Figure 8.

Tumors from mice treated with our nanoformulations (Figure 9c,d) exhibited notable histological differences from tumors of mice treated with pristine PTX and mice that received PBS. Accordingly, areas of degeneration were present in the tumors (red arrows), more apparent in tumors from mice that received the CTT nanosystem, amounting to over 60% of the mass. Moreover, a significant decline in the mitosis count was recorded, with only 10 and 5 mitosis present in tumors from mice that received CLA-coated PTX-SPIONs and CTT nanosystem, respectively. The low mitosis counts recorded from treatments with our nanoformulations could be attributed to the enhanced activity of PTX as an antimitotic agent, when in nanoformulation rather than in pristine form. The significant degeneration of neoplastic cells arising from treatment with the CTT nanosystem could be linked to the inhibition of angiogenesis through MMP-2 arrest by the nanoformulation, which limited the formation of new blood vessels and meant that neoplastic cells could no longer get nourishment (i.e., oxygen and essential nutrients) required for growth and ended up deteriorating. In essence, this supports the notion that MMP-2 is an important factor in the promotion of tumor angiogenesis.

Pharmacokinetics Profile of PTX in Plasma. Pharmacokinetics (PK) evaluation was carried out to assess the absorption and circulation profiles of PTX when in the CLA-coated PTX-SPIONs@CTT nanoformulation. Essentially, an ideal nanomedicine should be able to afford the active pharmaceutical ingredient's adequate absorption circulation time in the body for eliciting desired therapeutic action.[53,54] Accordingly, single SC injections of the CTT nanosystem and comparator Taxol were administered in mice, and PTX concentrations were quantified from plasma. The PK profile is shown in Figure 10, and PK parameters are listed in Table 3. A relatively high plasma concentration of 19.7 μg/mL was recorded at 0.5 h of Taxol injection; meanwhile, 15.2 μg/mL was recorded at the same time point for CLA-coated PTX-SPIONs@CTT. This suggested that PTX in the nano-

https://doi.org/10.1021/acsomega.3c06489
ACS Omega 2024, 9, 700−713

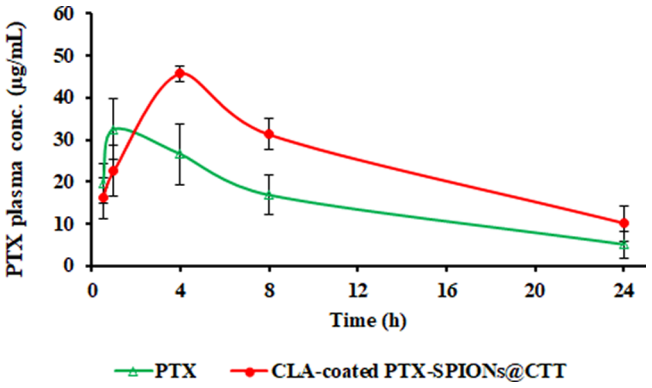

Figure 10. PK profile of PTX from plasma following a single SC administration of commercial Taxol and our formulated CTT nanosystem. Data are shown as mean ± SD, $n = 3$.

Table 3. PK Parameters of PTX from Taxol and the CTT Nanosystem in Plasma[a]

	C_{max} (μg/mL)	T_{max} (h)	$T_{1/2}$ (h)	K_{el} (h^{-1})	AUC_{0-24} (μg/mL.h)
CTT nanosystem	48.8 ± 4.3	4.0	16.8	0.04	659.6
Taxol	32.5 ± 3.7	1.0	9.0	0.07	365.4

[a] K_{el}, elimination rate constant; AUC_{0-24}, area under the curve (concentration vs time).

formulation is slowly released and absorbed into plasma when injected subcutaneously, which correlates with the demonstrated sustained release in vitro.

Furthermore, comparator PTX reached the maximal plasma concentration (C_{max}) of 32.5 μg/mL at 1 h, whereas from our nanosystem, a C_{max} of 48.8 μg/mL was recorded at 4 h. These corresponded with a half-life ($T_{1/2}$) of 8.9 h from Taxol and $T_{1/2}$ = 16.8 h from CLA-coated PTX-SPIONs@CTT. The prolonged half-life and higher C_{max} recorded for PTX from the nanosystem exhibited the ability of the nanosystem to limit the exposure of PTX to nonspecific binding and presystemic degradation. Essentially, PTX is known to present with nonspecific protein binding, enzymatic degradation, and rapid clearance, which affect its bioavailability.[3] Moreover, the current commercial Taxol enhancer (Cremophor EL; polyoxyethylated castor oil and anhydrous alcohol) presents further undesired side effects which need to be averted.[55] Therefore, the formulated CLA-coated PTX-SPIONs@CTT presents a promising PTX delivery nanosystem as a potential nanomedicine for NSCLC management.

CONCLUSIONS

A targeted PTX delivery nanosystem with anti-MMP-2 activity was successfully formulated, and it exhibited suitable characteristics for potential application as a potent nanovector of PTX with tumor targetability in NSCLC. A safe-by-design methodology was established to achieve efficient conjugation of the CTT peptide on surface-modified SPIONs. The formulated CTT nanosystem exhibited high PTX adsorption efficiency, site-specific sustained in vitro PTX release, enhanced PTX antiproliferative activity, and excellent cellular uptake for potential application as a nanomedicine in NSCLC therapy. The nanosystem possesses active tumor targetability and antiangiogenic activity, as supported by a tumor growth inhibition of 69.7% resulting from neoplastic cell degeneration in vivo, owing to possible angiogenesis inhibition.

Moreover, the nanosystem depicted a relatively improved half-life of PTX and prolonged its plasma circulation time following SC administration. In essence, our formulated CTT nanosystem exhibits relatively stronger physicochemical properties (i.e., <100 nm particle size, 98.5% drug adsorption efficiency, and aqueous stability) and favorable therapeutic attributes (considering the low dosages employed) compared to some reported PTX delivery polymeric nanoparticles designed for NSCLC.[54,56,57] Accordingly, the in vitro and in vivo merits displayed make the nanosystem a potential alternative candidate for targeted nanotherapy in NSCLC. Additionally, the magnetic core of the nanosystem, which is known to have imaging benefits, could be explored in the future for potential theragnostic application in NSCLC therapy for guided magnetic resonance imaging to provide precise diagnosis and treatment.

EXPERIMENTAL SECTION

Materials. Iron precursors comprising iron(II) chloride tetrahydrate ($FeCl_2{\cdot}4H_2O$) and (III) chloride hexahydrate ($FeCl_3{\cdot}6H_2O$), reagents, conjugated (10E, 12Z)-linoleic acid ethanol solution, DMSA, *N*-hydroxysuccinimide (NHS), 1-ethyl-3(3-(dimethylamino)propyl) carbodiimide (EDC), FITC, paclitaxel (Taxol), and solvents and general chemicals, dimethyl sulfoxide (DMSO), DMF, PBS tablets, and sodium hydroxide (NaOH) were procured from Sigma-Aldrich Corp. (St. Louis, MO, USA). The CTT peptide (95% purity) was acquired from Peptron Inc. (Daejeon, South Korea). All solvents were of analytical standard and utilized as obtained.

Formulation of CLA-Coated PTX-SPIONs. CLA-coated PTX-SPIONs were formulated using an established method by Ngema et al.[20] Briefly, SPIONs were synthesized via a coprecipitation technique from an aqueous solution of $FeCl_2{\cdot}4H_2O$ (0.3 mol) and $FeCl_3{\cdot}6H_2O$ (0.6 mol) under an inert (N_2) atmosphere. Following was the coating of SPIONs with 10E, 12Z CLA in a single-step reaction, and the CLA content on SPIONs was quantified by TGA (TGA 4000, PerkinElmer Inc., Waltham, MA, USA).[20] PTX was efficiently loaded by self-assembling onto CLA via spontaneous CLA∼PTX hydrophobic interaction, facilitating PTX adsorption on the CLA hydrophobic ends. The amount of PTX used for loading was fixed at 10% w/w of the nanoparticles. The %AE of PTX and the %DLC of the nanosystem were determined using UV spectrophotometry (Cary 50, Varian Inc., Palo Alto, CA, USA). Briefly, following an established and direct method,[58] the nanosystem was completely air-dried and vigorously ruptured by probe sonication in 5 mL of 70% methanol and filtered for UV quantification at 227 nm, and computation of % AE and %DLC was performed using formulas 1 and 2, respectively[20,58]:

$$\%\mathrm{AE} = \frac{D_q}{D_l} \times 100 \quad (1)$$

$$\%\mathrm{DLC} = \frac{D_q}{W_f} \times 100 \quad (2)$$

where D_q denotes the amount of drug as quantified by UV spectrophotometry, D_l is the amount of drug initially loaded, and W_f is the overall weight of formulation in mg.

https://doi.org/10.1021/acsomega.3c06489
ACS Omega 2024, 9, 700−713

Carboxylic Acid Functionalization of CLA-Coated PTX-SPIONs. Following a functionalization step by Dilnawaz et al.,[24] the method with adjustments was carried out for the surface functionalization of CLA-coated PTX-SPIONs. This involved the addition of carboxylic acid (COOH) groups to the surface of the SPIONs to aid the conjugation of the CTT peptide. Accordingly, CLA-coated PTX-SPIONs (15 mg) were mixed with 500 μL of 1.6 M DMSA dissolved in DMF and kept under continuous magnetic stirring (MSH10, Labcon, Mogale City, SA) for 20 h. The resulting suspension was subjected to centrifugation (~14,000 rpm, 10 °C) on a TC-MiniSpin Centrifuge (TopScien, Ningbo, China) for 30 min and washed three times with ethanol. The resultant pellet was lyophilized and analyzed on a FT-IR spectrometer (Spectrum 100, PerkinElmer Inc., Waltham, MA, USA) to confirm functionalization, and double-titration was performed to work out acid numbers.[24]

Conjugation of CTT to CLA-Coated PTX-SPIONs. CTT peptide was conjugated to carboxylic acid-bound CLA-coated PTX-SPIONs using EDC and NHS (EDC/NHS chemistry).[8,24,59] Briefly, 10 mg of COOH-bound CLA-coated PTX-SPIONs was added into 5 mL of PBS (0.01 M, pH 7.4). EDC and NHS solutions (1 mg/mL in PBS, pH 7.4) were constituted, and 250 μL of each was introduced into the sample. The reaction was allowed to proceed with stirring (200 rpm) at ambient temperature for 4 h and precipitated with a permanent magnet. The supernatant was decanted, and 2 mL of PBS (0.01 M, pH 7.4) and 200 μL of CTT (1 mg/mL) were added into the pellet and left for 2 h at room temperature before overnight incubation at 4 °C. Thereafter, upon use of a magnet, the supernatant was withdrawn, and the resulting pellet was washed three times with PBS to remove and determine the unbound peptide. The resultant CLA-coated PTX-SPIONs@CTT was air-dried at ambient temperature, and CTT conjugation was confirmed by FT-IR spectroscopy.

Analysis of Chemical Structural Transformations. Comparative FT-IR spectra of the formulated CTT nanosystem and precursors were recorded and used to infer any changes in the structural integrity and to identify functional transformations on the components of the CTT nanosystem. All spectra were acquired over 20 scans from 4000 to 550 cm^{-1} at 100 psi pressure.

Determination of Size, Surface Charge, and Overall Morphology of the CTT Nanosystem. The surface charge and hydrodynamic size of CLA-coated PTX-SPIONs@CTT were confirmed by a ZetaSizer (Malvern NanoZS, Panalytical, Malvern, UK) using a dried sample (10 μg) suspended in distilled water (1 mL). The suspension was sonicated for 5 min before analysis at 25 °C. The hydrodynamic size and PDI were recorded using a disposable cuvette, and zeta potential was measured using a special DTS 1070 cuvette. The same sample was used (aliquot) to ascertain the morphology of the CTT nanosystem using TEM (FEI Tecnai T12, FEI Technologies Inc., Hillsboro, OR, USA). A mounting copper grid (200 mesh with carbon coating) was dipped in the sample and allowed to dry for TEM analysis.

In Vitro Analysis of PTX Release from the CTT Nanosystem. In vitro release of PTX from the CTT nanosystem was investigated over 24 h at pH 6.8 and physiological pH 7.4.[8] A suspension of 3 mg of previously dried CTT nanosystem in buffer solutions (2.5 mL, 0.1 M; 0.1% v/v tween) was pipetted into the SnakeSkin dialysis membrane (3 500 MWCO). The dialysis membrane was submerged in 30 mL of the respective release buffer (pH 6.8 and 7.4). The samples were incubated in an orbital shaker (LM-530, YIHDER Co., Ltd., Taipei, Taiwan) at 37 °C, with sampling done over a 24 h interval at t = 1, 2, 4, 8, 12, 16, and 24 h. The sampled volume (2 mL) was analyzed with a UV spectrophotometer (Cary 50, Varian Inc., Palo Alto, CA, USA) at 227 nm (PTX absorbance), and the medium was replenished with 2 mL after each sampling.

Evaluation of Antiproliferative Action on A549 Cancer Cells. A general protocol for cell culturing was applied to culture lung adenocarcinoma (A549) cells for the study.[20] Accordingly, a growth medium comprising Dulbecco's modified Eagle medium, fetal bovine serum (FBS, 10% v/v), and 1% v/v penicillin-streptomycin antibiotic was prepared for growing the cells in a T-25 culture flask at 37 °C and 5% CO_2 in a humidified incubator. Cells were allowed to grow to 90% confluence and then seeded (2.5×10^4 cells/mL, 90 μL each well) in a 96-well plate and adhered under incubation for over 24 h. Subsequently, the test cells were dosed with 10 μL of varying concentrations (i.e., 25, 50, and 100 μg/mL) of CLA-coated PTX-SPIONs@CTT in triplicate prepared in PBS (0.2% DMSO). Likewise, control cells were treated with corresponding concentrations of pristine PTX in 0.2% DMSO in PBS. Thereafter, the cells were incubated for 72 h for cell viability assessment using a 3-(4,5-dimethylthiazole-2-yl)-2,5-diphenyl tetrazolium bromide (MTT) assay (MTT Cell Proliferation Kit I, Roche, Basel, Switzerland). As per a standard MTT protocol, each well was filled with 10 μL of MTT solution (5 mg/mL), and the plate was further incubated at 37 °C, 5% CO_2 for 4 h. A solution of acid-isopropanol solubilizing agent (100 μL) was introduced to dissolve the formazan crystals, and the plates were subjected to overnight incubation (37 °C and 5% CO_2). The results were recorded on a multiplate analyzer (Victor X3, PerkinElmer, Waltham, MA, USA) at 570 and 620 nm reference wavelengths. The absorbance readings were used to determine % cell viability (CV) from eq 3. Blank wells contained only growth medium and solubilizing agent. The IC_{50} values were generated using the standard ATT Bioquest IC_{50} calculator.

$$\%\mathrm{CV} = \frac{A_{\mathrm{test}} - A_{\mathrm{blank}}}{A_{\mathrm{control}} - A_{\mathrm{blank}}} \times 100 \tag{3}$$

where A_{test}, A_{control}, and A_{blank} are absorbance from test, control, and blank wells in nm.

Assessment on Uptake and Internalization by A549 Cells. The cellular uptake and internalization of the CTT nanosystem was evaluated using an FITC-labeled nanoformulation. FITC labeling was achieved through a methodology of Kumar and Srivastava (2018), with modifications.[60] Accordingly, 1 mg/mL FITC solution was consituted in methanol: dichloromethane (50:50) and added into a 5 mL suspension of 2.5 mg of CTT nanosystem in distilled water. The sample was allowed to continuously stir, and the solvent was evaporated in the dark for 20 min at room temperature. Subsequently, the sample was washed by centrifugation (×3 distilled water) for 15 min at 14 000 rpm and 10 °C (MiniSpin TC Centrifuge, TopScien, Ningbo, China). FITC-labeled CTT nanosystem was collected for cell work. The nonfunctionalized nanosystem was similarly labeled with FITC and compared with the CTT nanosystem.

Following a standard cell culture protocol, A549 cells were cultured and seeded in a 6-well plate at 5×10^4 cells/mL

https://doi.org/10.1021/acsomega.3c06489
ACS Omega 2024, 9, 700−713

seeding density. The wells were fitted with presterilized coverslips, and each contained 800 μL of cell suspension. The cells were incubated for 24 h, followed by treatment with a FITC-CTT nanosystem (200 μL of 1 mg/mL in PBS) and further 24 h incubation at 37 °C and 5% CO_2. Subsequently, the cells were spiked with 500 μL of paraformaldehyde (PFA, 4%) for 3 min for cell acclimatization. Thereafter, the well contents were aspirated, a further 1 mL 4% PFA was added per well, and the cells were incubated for 20 min for cell fixation. The fixed cells were washed with 1× PBS (2 mL, four times) before staining with 300 μL of DAPI (300 nM) and incubating in the dark at room temperature for 5 min. Further four washes with 1XPBS were done before the coverslips were removed and fixed on glass slides using cool glycerol (80% v/v) and allowed to dry overnight. The slides were then analyzed on an Olympus IX51 fluorescent microscope, super 40X objective (Olympus Corporation, Tokyo, Japan), with images captured at 517 and 416 nm for FITC green fluorescence excitation and DAPI (blue fluorescence), respectively.

Evaluation of MMP-2 Targeting Activity. An Invitrogen human MMP-2 ELISA kit was employed to assess the binding ability of CLA-coated PTX-SPIONs@CTT onto MMP-2 on HMEC-1. A typical MCDB 131 medium with special supplements of 10% v/v FBS, 1 μg/mL hydrocortisone, 10 ng/mL human EGF recombinant protein, and 10 nM L-glutamine was used to culture HMEC-1 cells in a T-25 flask. The cells were cultured at 37 °C, 5% CO_2 until 90% confluence, and 800 μL of cells were seeded in two 6-well plates at a seeding density of 5×10^4 cells/mL and allowed 24 h to adequately adhere. A concentration of 50 μg/mL CTT nanosystem, CLA-coated PTX-SPIONs, and pristine CTT was used to treat the experimental cells for 24 h. Post 24 h incubation, the cell culture supernatant was collected and immediately subjected to centrifugation for 20 min at 14,000, 4 °C (Eppendorf 5415R, Merck, Darmstadt, Germany). The ELISA analysis was conducted using the supernatant, following the manufacturer's protocol. A Victor X3 multimodal microplate analyzer was utilized to read the absorbance at 450 nm.

Establishment of Subcutaneous Lung Tumor Xenograft Model. Female Athymic nude mice (MF1-nu/nu; 4−6 weeks old; 18−22 g) were acquired with approval from the University of the Witwatersrand's Animal Research Screening Committee, ethical certification number 2020/11/01/B. Mice were first anaesthetized with isoflurane gas (2% in oxygen) and then subcutaneously injected with 3.9×10^5 A549 lung cancer cells in PBS at the right flank, with each mouse receiving 50 μL of the suspension. The mice were housed under controlled temperature and humidity on a 12 h light/dark cycle with food and water provided ad libitum. Tumors developed after 20 days and were routinely measured using a digital caliper until the desired volume (90−100 mm^3) was reached and treatment could commence.

Evaluation of Antitumor Activity of the CTT Nanosystem. Mice with solid tumors were treated with prepared doses of the CTT nanosystem, CLA-coated PTX-SPIONs, and a comparator PTX (Taxol), while a placebo group received only PBS. Mice were randomly grouped into four groups (n = 3) and injected (SC; 20 mm away from tumor) with 100 μL corresponding to a dosage of 12 mg/kg CTT nanosystem, CLA-coated PTX-SPIONs, and 1.2 mg/kg Taxol (tolerated dose corresponding to 10% PTX in our formulation, accounting for ∼10% DLC). Meanwhile, a placebo group received 100 μL of PBS. The sample size (n = 3 per group) was adopted from previous reports[10,61] to adhere to ethical regulations and obtain reliable and statistically sound data. Mice received injections every 4 days on days 0, 4, 8, and 12.[49] Tumor volumes and animal weight were measured before every treatment cycle and every 4 days after each cycle until the last day of the study (day 20). Tumor growth inhibition rate (%TGI), measured relative to the control/placebo group, was determined at the end of the study. On day 20, the mice were humanely euthanized and tumors excised for further analysis.

Tumor Histopathological Assessment. Excised tumors were timely placed in 10% neutral buffered formalin and thereafter carefully transferred into paraffin for sectioning (4−5 μm). The tissues were stained with hematoxylin and eosin (H&E staining), and histology analysis was conducted.[36]

Plasma PK. Mice were randomly grouped into three groups (n = 3) and accordingly received a single SC injection of 12 mg/kg CTT nanosystem, 1.2 mg/kg Taxol, and 100 μL PBS for the control group. Mice were humanely euthanized at different time points, namely, t = 0.5, 1, 4, 8, and 24 h. Blood was acquired via cardiac puncture into microcentrifuge tubes flushed with heparin, then centrifuged at 11,000 rpm for 15 min, 10 °C (MiniSpin TC Centrifuge, TopScien, Ningbo, China), and plasma collected for extraction and high-pressure liquid chromatography (HPLC) analysis (Flexar LC UV/vis, PerkinElmer Inc., Waltham, MA, USA). A liquid−liquid extraction method was adopted, and samples were analyzed using a validated HPLC method.[62]

Statistical Analysis. GraphPad prism 9 was utilized to perform two-tailed Student's t-test for data analysis (GraphPad Software, Inc., San Diego, CA, USA). Criteria for statistically significant data were set at $p < 0.05$. Data collected for three data points (n = 3) are represented as mean values ± standard deviation.

AUTHOR INFORMATION

Corresponding Author

Yahya E. Choonara − *Wits Advanced Drug Delivery Platform Research Unit, Department of Pharmacy and Pharmacology, School of Therapeutic Sciences, Faculty of Health Sciences, University of the Witwatersrand, Johannesburg 2193, South Africa;* orcid.org/0000-0002-3889-1529; Phone: +27 11 717 2052; Email: yahya.choonara@wits.ac.za

Authors

Lindokuhle M. Ngema − *Wits Advanced Drug Delivery Platform Research Unit, Department of Pharmacy and Pharmacology, School of Therapeutic Sciences, Faculty of Health Sciences, University of the Witwatersrand, Johannesburg 2193, South Africa*

Samson A. Adeyemi − *Wits Advanced Drug Delivery Platform Research Unit, Department of Pharmacy and Pharmacology, School of Therapeutic Sciences, Faculty of Health Sciences, University of the Witwatersrand, Johannesburg 2193, South Africa*

Thashree Marimuthu − *Wits Advanced Drug Delivery Platform Research Unit, Department of Pharmacy and Pharmacology, School of Therapeutic Sciences, Faculty of Health Sciences, University of the Witwatersrand, Johannesburg 2193, South Africa;* orcid.org/0000-0003-1487-5273

Philemon N. Ubanako − *Wits Advanced Drug Delivery Platform Research Unit, Department of Pharmacy and*

https://doi.org/10.1021/acsomega.3c06489
ACS Omega 2024, 9, 700−713

Pharmacology, School of Therapeutic Sciences, Faculty of Health Sciences, University of the Witwatersrand, Johannesburg 2193, South Africa

Wilfred Ngwa − *Sidney Kimmel Comprehensive Cancer Center, Johns Hopkins Medicine, Baltimore, Maryland 21218, United States*

Complete contact information is available at: https://pubs.acs.org/10.1021/acsomega.3c06489

Author Contributions

The listed authors have all contributed to the preparation of the manuscript and have approved the current version of the manuscript.

Funding

Friedel Sellschop Grant from the University of the Witwatersrand, Johannesburg, and SARChI Grant from the National Research Foundation (NRF), Pretoria, South Africa.

Notes

The authors declare no competing financial interest.

■ ACKNOWLEDGMENTS

The authors are thankful for the Friedel Sellschop Grant from the University of the Witwatersrand, Johannesburg and the SARChI Grant from the National Research Foundation (NRF), Pretoria, South Africa for their financial support.

■ ABBREVIATIONS

10E,12Z, *trans*-10,*cis*-12; CLA, conjugated linoleic acid; CTT, CTTHWGFTLC; CTT nanosystem, CLA-coated PTX-SPIONs@CTT; DMSA, *meso*-2,3-Dimercaptosuccinic acid; DTX, docetaxel; HMEC-1, human dermal microvascular endothelial cell line; PTX, paclitaxel; SPIONs, superparamagnetic iron oxide nanoparticles

■ REFERENCES

(1) Salehi, M.; Movahedpour, A.; Tayarani, A.; Shabaninejad, Z.; Pourhanifeh, M. H.; Mortezapour, E.; Nickdasti, A.; Mottaghi, R.; Davoodabadi, A.; Khan, H.; Savardashtaki, A.; Mirzaei, H. Therapeutic Potentials of Curcumin in the Treatment of Non-Small-Cell Lung Carcinoma. *Phytother. Res.* **2020**, *34*, 2557−2576.

(2) Ngema, L. M.; Adeyemi, S. A.; Marimuthu, T.; Choonara, Y. E. A Review on Engineered Magnetic Nanoparticles in Non-Small-Cell Lung Carcinoma Targeted Therapy. *Int. J. Pharm.* **2021**, *606*, No. 120870.

(3) Ye, Z.; Huang, Y.; Ke, J.; Zhu, X.; Leng, S.; Luo, H. Breakthrough in Targeted Therapy for Non-Small Cell Lung Cancer. *Biomed. Pharmacother.* **2021**, *133*, No. 111079.

(4) Genova, C.; Rossi, G.; Tagliamento, M.; Rijavec, E.; Biello, F.; Cerbone, L.; Zullo, L.; Grossi, F. Targeted Therapy of Oncogenic-Driven Advanced Non-Small Cell Lung Cancer: Recent Advances and New Perspectives. *Expert Rev. Respir. Med.* **2020**, *14*, 367−383.

(5) Shukla, N. A.; Yan, M. N.; Hanna, N. The Story of Angiogenesis Inhibitors in Non−small-Cell Lung Cancer: The Past, Present, and Future. *Clin. Lung Cancer* **2020**, *21*, 308−313.

(6) Lugano, R.; Ramachandran, M.; Dimberg, A. Tumor Angiogenesis: Causes, Consequences, Challenges and Opportunities. *Cell. Mol. Life Sci.* **2020**, *77*, 1745−1770.

(7) Bałan, B. J.; Siwicki, A. K.; Pastewka, K.; Demkow, U.; Skopiński, P.; Skopińska-Różewska, E.; Lewicki, S.; Zdanowski, R. Synergistic Activity for Natural and Synthetic Inhibitors of Angiogenesis Induced by Murine Sarcoma L-1 and Human Kidney Cancer Cells. *Adv. Exp. Med. Biol.* **2017**, *1020*, 91−104.

(8) Adeyemi, S. A.; Choonara, Y. E.; Kumar, P.; du Toit, L. C.; Marimuthu, T.; Kondiah, P. P. D.; Pillay, V. Folate-Decorated, Endostatin-Loaded Nanoparticles for Anti-Proliferative Chemotherapy in Esophaegeal Squamous Cell Carcinoma. *Biomed. Pharmacother.* **2019**, *119*, No. 109450.

(9) Lu, L.; Chen, H.; Hao, D.; Zhang, X.; Wang, F. The Functions and Applications of A7R in Anti-Angiogenic Therapy, Imaging and Drug Delivery Systems. *Asian J. Pharm. Sci.* **2019**, *14*, 595−608.

(10) Adeyemi, S. A.; Choonara, Y. E. In Vitro and In Vivo Evaluation of a Cyclic LyP-1-Modified Nanosystem for Targeted Endostatin Delivery in a KYSE-30 Cell Xenograft Athymic Nude Mice Model. *Pharmaceuticals* **2022**, *15*, 353.

(11) Quintero-Fabián, S.; Arreola, R.; Becerril-Villanueva, E.; Torres-Romero, J. C.; Arana-Argáez, V.; Lara-Riegos, J.; Ramírez-Camacho, M. A.; Alvarez-Sánchez, M. E. Role of Matrix Metalloproteinases in Angiogenesis and Cancer. *Front. Oncol.* **2019**, *9*, 1370.

(12) Han, L.; Sheng, B.; Zeng, Q.; Yao, W.; Jiang, Q. Correlation Between MMP2 Expression in Lung Cancer Tissues and Clinical Parameters: A Retrospective Clinical Analysis. *BMC Pulm. Med.* **2020**, *20*, 283−283.

(13) Gonzalez-Avila, G.; Sommer, B.; Mendoza-Posada, D. A.; Ramos, C.; Garcia-Hernandez, A. A.; Falfan-Valencia, R. Matrix Metalloproteinases Participation in the Metastatic Process and their Diagnostic and Therapeutic Applications in Cancer. *Crit. Rev. Oncol. Hematol.* **2019**, *137*, 57−83.

(14) Winkler, J.; Abisoye-Ogunniyan, A.; Metcalf, K. J.; Werb, Z. Concepts of Extracellular Matrix Remodelling in Tumour Progression and Metastasis. *Nat. Commun.* **2020**, *11*, 5120.

(15) Wang, H.; Yang, Z.; Gu, J. Therapeutic Targeting of Angiogenesis with a Recombinant CTT Peptide−Endostatin Mimic−Kringle 5 Protein. *Mol. Cancer Ther.* **2014**, *13*, 2674−2687.

(16) Ndinguri, M. W.; Bhowmick, M.; Tokmina-Roszyk, D.; Robichaud, T. K.; Fields, G. B. Peptide-Based Selective Inhibitors of Matrix Metalloproteinase-Mediated Activities. *Molecules* **2012**, *17*, 14230−14248.

(17) Webb, A. H.; Gao, B. T.; Goldsmith, Z. K.; Irvine, A. S.; Saleh, N.; Lee, R. P.; Lendermon, J. B.; Bheemreddy, R.; Zhang, Q.; Brennan, R. C.; Johnson, D.; Steinle, J. J.; Wilson, M. W.; Morales-Tirado, V. M. Inhibition of MMP-2 and MMP-9 Decreases Cellular Migration, and Angiogenesis in In Vitro Models of Retinoblastoma. *BMC Cancer* **2017**, *17*, 434−434.

(18) Penate Medina, O.; Haikola, M.; Tahtinen, M.; Simpura, I.; Kaukinen, S.; Valtanen, H.; Zhu, Y.; Kuosmanen, S.; Cao, W.; Reunanen, J.; Nurminen, T.; Saris, P. E. J.; Smith-Jones, P.; Bradbury, M.; Larson, S.; Kairemo, K. Liposomal Tumor Targeting in Drug Delivery Utilizing MMP-2- and MMP-9-Binding Ligands. *J. Drug Delivery* **2011**, *2011*, No. 160515.

(19) Holder, J. E.; Ferguson, C.; Oliveira, E.; Lodeiro, C.; Trim, C. M.; Byrne, L. J.; Bertolo, E.; Wilson, C. M. The Use of Nanoparticles for Targeted Drug Delivery in Non-Small Cell Lung Cancer. *Front. Oncol.* **2023**, *13*, No. 1154318.

(20) Ngema, L. M.; Adeyemi, S. A.; Marimuthu, T.; Ubanako, P.; Wamwangi, D.; Choonara, Y. E. Synthesis of Novel Conjugated Linoleic Acid (CLA)-Coated Superparamagnetic Iron Oxide Nanoparticles (SPIONs) for the Delivery of Paclitaxel with Enhanced In Vitro Anti-Proliferative Activity on A549 Lung Cancer Cells. *Pharmaceutics* **2022**, *14*, 829.

(21) Nana, A. B. A.; Marimuthu, T.; Kondiah, P. P. D.; Choonara, Y. E.; Du Toit, L. C.; Pillay, V. Multifunctional Magnetic Nanowires: Design, Fabrication, and Future Prospects as Cancer Therapeutics. *Cancers* **2019**, *11*, 1956.

(22) Dachev, M.; Bryndová, J.; Jakubek, M.; Moučka, Z.; Urban, M. The Effects of Conjugated Linoleic Acids on Cancer. *Processes* **2021**, *9*, 454.

(23) Slimani, S.; Meneghini, C.; Abdolrahimi, M.; Talone, A.; Murillo, J. P. M.; Barucca, G.; Yaacoub, N.; Imperatori, P.; Illés, E.; Smari, M.; Dhahri, E.; Peddis, D. Spinel Iron Oxide by the Co-Precipitation Method: Effect of the Reaction Atmosphere. *Appl. Sci.* **2021**, *11*, 5433.

(24) Dilnawaz, F.; Singh, A.; Mohanty, C.; Sahoo, S. K. Dual Drug Loaded Superparamagnetic Iron Oxide Nanoparticles for Targeted Cancer Therapy. *Biomaterials* **2010**, *31*, 3694−3706.
(25) Muzio, G.; Miola, M.; Ferraris, S.; Maggiora, M.; Bertone, E.; Puccinelli, M. P.; Ricci, M.; Borroni, E.; Canuto, R. A.; Verné, E.; Follenzi, A. Innovative Superparamagnetic Iron-Oxide Nanoparticles Coated with Silica and Conjugated with Linoleic Acid: Effect on Tumor Cell Growth and Viability. *Mater. Sci. Eng: C* **2017**, *76*, 439−447.
(26) Sawisai, R.; Wanchanthuek, R.; Radchatawedchakoon, W.; Sakee, U. Simple Continuous Flow Synthesis of Linoleic and Palmitic Acid-Coated Magnetite Nanoparticles. *Surf. Interfaces* **2019**, *17*, No. 100344.
(27) Kovrigina, E.; Chubarov, A.; Dmitrienko, E. High Drug Capacity Doxorubicin-Loaded Iron Oxide Nanocomposites for Cancer Therapy. *Magnetochemistry* **2022**, *8*, 54.
(28) Chen, T.; Jiang, Y.; Wang, C.; Cai, Z.; Chen, H.; Zhu, J.; Tao, P.; Wu, M. The pH-Triggered Drug Release and Simultaneous Carrier Decomposition of Effervescent SiO_2−Drug−Na_2CO_3 Composite Nanoparticles: to Improve the Antitumor Activity of Hydrophobic Drugs. *RSC Adv.* **2021**, *11*, 5335−5347.
(29) Bucholz, T. L.; Loo, Y.-L. Polar Aprotic Solvents Disrupt Interblock Hydrogen Bonding and Induce Microphase Separation in Double Hydrophilic Block Copolymers of PEGMA and PAAMPSA. *Macromolecules* **2008**, *41*, 4069−4070.
(30) Pochapski, D. J.; Carvalho dos Santos, C.; Leite, G. W.; Pulcinelli, S. H.; Santilli, C. V. Zeta Potential and Colloidal Stability Predictions for Inorganic Nanoparticle Dispersions: Effects of Experimental Conditions and Electrokinetic Models on the Interpretation of Results. *Langmuir* **2021**, *37*, 13379−13389.
(31) Gonçalves, L. C.; Seabra, A. B.; Pelegrino, M. T.; de Araujo, D. R.; Bernardes, J. S.; Haddad, P. S. Superparamagnetic Iron Oxide Nanoparticles Dispersed in Pluronic F127 Hydrogel: Potential Uses in Topical Applications. *RSC Adv.* **2017**, *7*, 14496−14503.
(32) Hoshyar, N.; Gray, S.; Han, H.; Bao, G. The Effect of Nanoparticle Size on In Vivo Pharmacokinetics and Cellular Interaction. *Nanomedicine* **2016**, *11*, 673−692.
(33) Song, L. N.; Gu, N.; Zhang, Y. A Moderate Method for Preparation of DMSA Coated Fe_3O_4 Nanoparticles. *IOP Conf. Ser.: Mater. Sci. Eng.* **2017**, *164*, No. 012026.
(34) Li, W.; Yu, H.; Ding, D.; Chen, Z.; Wang, Y.; Wang, S.; Li, X.; Keidar, M.; Zhang, W. Cold Atmospheric Plasma and Iron Oxide-Based Magnetic Nanoparticles for Synergetic Lung Cancer Therapy. *Free Radic. Biol. Med.* **2019**, *130*, 71−81.
(35) Eid, M. M. Characterization of Nanoparticles by FTIR and FTIR-Microscopy. In *Handbook of Consumer Nanoproducts*; Mallakpour, S., Hussain, C. M., Eds.; Springer: Singapore, 2021; pp 1−30.
(36) Ngema, L. M.; Adeyemi, S. A.; Marimuthu, T.; Ubanako, P. N.; Ngwa, W.; Choonara, Y. E. Surface Immobilization of Anti-VEGF Peptide on SPIONs for Antiangiogenic and Targeted Delivery of Paclitaxel in Non-Small-Cell Lung Carcinoma. *ACS Appl. Bio Mater.* **2023**, *6*, 2747−2759.
(37) Akilo, O. D.; Choonara, Y. E.; Strydom, A. M.; du Toit, L. C.; Kumar, P.; Modi, G.; Pillay, V. An In Vitro Evaluation of a Carmustine-Loaded Nano-co-Plex for Potential Magnetic-Targeted Intranasal Delivery to the Brain. *Int. J. Pharm.* **2016**, *500*, 196−209.
(38) Çitoğlu, S.; Coşkun, Ö. D.; Tung, L. D.; Onur, M. A.; Thanh, N. T. K. DMSA-Coated Cubic Iron Oxide Nanoparticles as Potential Therapeutic Agents. *Nanomedicine* **2021**, *16*, 925−941.
(39) Tsoukalas, C.; Psimadas, D.; Kastis, G. A.; Koutoulidis, V.; Harris, A. L.; Paravatou-Petsotas, M.; Karageorgou, M.; Furenlid, L. R.; Moulopoulos, L. A.; Stamopoulos, D.; Bouziotis, P. A Novel Metal-Based Imaging Probe for Targeted Dual-Modality SPECT/MR Imaging of Angiogenesis. *Front. Chem.* **2018**, *6*, 224.
(40) Rinawati, L.; Nugraha, R. E.; Mahdia, R.; Munifa, I.; Chasanah, U.; Wahyuningsih, S.; Ramelan, A. Increasing the Effectiveness of Pesticides Based Urea Nanofertilizer Encapsulated Nanosilica with Addition of Rice Husk TiO_2 Additive Substances. *J. Chem. Pharm. Res.* **2015**, *7*, 85−89.
(41) Wulandari, I. O.; Sulistyarti, H.; Safitri, A.; Santjojo, D.; Sabarudin, A. Development of Synthesis Method of Magnetic Nanoparticles Modified by Oleic Acid and Chitosan as a Candidate for Drug Delivery Agent. *J. Appl. Pharm. Sci.* **2019**, *9*, 1−11.
(42) Engelberg, S.; Netzer, E.; Assaraf, Y. G.; Livney, Y. D. Selective Eradication of Human Non-Small Cell Lung Cancer Cells Using Aptamer-Decorated Nanoparticles Harboring a Cytotoxic Drug Cargo. *Cell Death Dis.* **2019**, *10*, 702.
(43) Foldbjerg, R.; Dang, D. A.; Autrup, H. Cytotoxicity and Genotoxicity of Silver Nanoparticles in the Human Lung Cancer Cell Line, A549. *Arch. Toxicol.* **2011**, *85*, 743−750.
(44) Jiang, L.; Li, X.; Liu, L.; Zhang, Q. Thiolated Chitosan-Modified PLA-PCL-TPGS Nanoparticles for Oral Chemotherapy of Lung Cancer. *Nanoscale Res. Lett.* **2013**, *8*, 66.
(45) Currie, E.; Schulze, A.; Zechner, R.; Walther, T. C.; Farese, R. V., Jr. Cellular Fatty Acid Metabolism and Cancer. *Cell Metab.* **2013**, *18*, 153−161.
(46) Shen, Q.; Lee, E. S.; Pitts, R. L.; Wu, M. H.; Yuan, S. Y. Tissue Inhibitor of Metalloproteinase-2 Regulates Matrix Metalloproteinase-2-Mediated Endothelial Barrier Dysfunction and Breast Cancer Cell Transmigration through Lung Microvascular Endothelial Cells. *Mol. Cancer Res.* **2010**, *8*, 939−951.
(47) Cabral-Pacheco, G. A.; Garza-Veloz, I.; Castruita-De la Rosa, C.; Ramirez-Acuña, J. M.; Perez-Romero, B. A.; Guerrero-Rodriguez, J. F.; Martinez-Avila, N.; Martinez-Fierro, M. L. The Roles of Matrix Metalloproteinases and Their Inhibitors in Human Diseases. *Int. J. Mol. Sci.* **2020**, *21*, 9739.
(48) Fares, J.; Fares, M. Y.; Khachfe, H. H.; Salhab, H. A.; Fares, Y. Molecular Principles of Metastasis: A Hallmark of Cancer Revisited. *Signal Transduct. Target. Ther.* **2020**, *5*, 28.
(49) Zou, Y.; Wei, J.; Xia, Y.; Meng, F.; Yuan, J.; Zhong, Z. Targeted Chemotherapy for Subcutaneous and Orthotopic Non-Small Cell Lung Tumors with Cyclic RGD-Functionalized and Disulfide-Crosslinked Polymersomal Doxorubicin. *Signal Transduct. Target. Ther.* **2018**, *3*, 32.
(50) Kim, S. C.; Kim, D. W.; Shim, Y. H.; Bang, J. S.; Oh, H. S.; Kim, S. W.; Seo, M. H. In Vivo Evaluation of Polymeric Micellar Paclitaxel Formulation: Toxicity and Efficacy. *J. Controlled Release* **2001**, *72*, 191−202.
(51) Zombeck, J. A.; Fey, E. G.; Lyng, G. D.; Sonis, S. T. A Clinically Translatable Mouse Model for Chemotherapy-Related Fatigue. *Comp. Med.* **2013**, *63*, 491−497.
(52) Zhao, H.; Wu, L.; Yan, G.; Chen, Y.; Zhou, M.; Wu, Y.; Li, Y. Inflammation and Tumor Progression: Signaling Pathways and Targeted Intervention. *Signal Transduct. Target. Ther.* **2021**, *6*, 263.
(53) Reichel, A.; Lienau, P. Pharmacokinetics in Drug Discovery: An Exposure-Centred Approach to Optimising and Predicting Drug Efficacy and Safety. In *New Approaches to Drug Discovery*; Nielsch, U., Fuhrmann, U., Jaroch, S., Eds.; Springer International Publishing, 2016; pp 235−260.
(54) Huang, G.; Zang, B.; Wang, X.; Liu, G.; Zhao, J. Encapsulated Paclitaxel Nanoparticles Exhibit Enhanced Anti-Tumor Efficacy in A549 Non-Small Lung Cancer Cells. *Acta Biochim. Biophys. Sin.* **2015**, *47*, 981−987.
(55) Gala, U. H.; Miller, D. A.; Williams, R. O. Harnessing the Therapeutic Potential of Anticancer Drugs Through Amorphous Solid Dispersions. *Biochim. Biophys. Acta* **2020**, *1873*, No. 188319.
(56) Pi, C.; Zhao, W.; Zeng, M.; Yuan, J.; Shen, H.; Li, K.; Su, Z.; Liu, Z.; Wen, J.; Song, X.; Lee, R. J.; Wei, Y.; Zhao, L. Anti-Lung Cancer Effect of Paclitaxel Solid Lipid Nanoparticles Delivery System with Curcumin as Co-Loading Partner In Vitro and In Vivo. *Drug Delivery* **2022**, *29*, 1878−1891.
(57) Yu, H.; Wang, Y.; Wang, S.; Li, X.; Li, W.; Ding, D.; Gong, X.; Keidar, M.; Zhang, W. Paclitaxel-Loaded Core-Shell Magnetic Nanoparticles and Cold Atmospheric Plasma Inhibit Non-Small Cell Lung Cancer Growth. *ACS Appl. Mater. Interfaces* **2018**, *10*, 43462−43471.

https://doi.org/10.1021/acsomega.3c06489
ACS Omega 2024, 9, 700−713

(58) Adekiya, T. A.; Kumar, P.; Kondiah, P. P. D.; Ubanako, P.; Choonara, Y. E. In Vivo Evaluation of Praziquantel-Loaded Solid Lipid Nanoparticles against S. mansoni Infection in Preclinical Murine Models. *Int. J. Mol. Sci.* **2022**, *23*, 9485.
(59) Pugliese, R.; Gelain, F. Cross-Linked Self-Assembling Peptides and Their Post-Assembly Functionalization via One-Pot and In Situ Gelation System. *Int. J. Mol. Sci.* **2020**, *21*, 4261.
(60) Kumar, P.; Srivastava, R. FITC Conjugated Polycaprolactone-Glycol-Chitosan Nanoparticles Containing The Longwave Emitting Fluorophore IR 820 for In Vitro Tracking Of Hyperthermia-Induced Cell Death. *bioRxiv* **2018**, *101*, 273748.
(61) Rodallec, A.; Sicard, G.; Giacometti, S.; Carré, M.; Pourroy, B.; Bouquet, F.; Savina, A.; Lacarelle, B.; Ciccolini, J.; Fanciullino, R. 3D Spheroids to Tumor Bearing Mice: Efficacy and distribution. *Int. J. Nanomed.* **2018**, *13*, 6677−6688.
(62) Rezazadeh, M.; Emami, J.; Mostafavi, A.; Rostami, M.; Hassanzadeh, F.; Sadeghi, H.; Minaiyan, M.; Lavasanifar, A. A Rapid and Sensitive HPLC Method for Quantitation of Paclitaxel in Biological Samples using Liquid-Liquid Extraction and UV Detection: Application to Pharmacokinetics and Tissues Distribution Study of Paclitaxel Loaded Targeted Polymeric Micelles in. *J. Pharm. Pharm. Sci.* **2015**, *18*, 647−660.

https://doi.org/10.1021/acsomega.3c06489
ACS Omega 2024, 9, 700−713